



LAWRENCE
LIVERMORE
NATIONAL
LABORATORY

Intrinsic superconductivity in layered van der Waals material PS2

Y. Li, E. Stavrou, Q. Zhu, S. M. Clarke, Y. Li, H.
Huang

January 7, 2019

Physical Review Letters

Disclaimer

This document was prepared as an account of work sponsored by an agency of the United States government. Neither the United States government nor Lawrence Livermore National Security, LLC, nor any of their employees makes any warranty, expressed or implied, or assumes any legal liability or responsibility for the accuracy, completeness, or usefulness of any information, apparatus, product, or process disclosed, or represents that its use would not infringe privately owned rights. Reference herein to any specific commercial product, process, or service by trade name, trademark, manufacturer, or otherwise does not necessarily constitute or imply its endorsement, recommendation, or favoring by the United States government or Lawrence Livermore National Security, LLC. The views and opinions of authors expressed herein do not necessarily state or reflect those of the United States government or Lawrence Livermore National Security, LLC, and shall not be used for advertising or product endorsement purposes.

Novel van der Waals layered compound PS₂ with superconductivity

Yan-Ling Li,^{1,*} Elissaios Stavrou,² Qiang Zhu,³ Samantha M. Clarke,² Yunguo Li,^{1,4} and Hong-Mei Huang¹

¹Laboratory for Quantum Design of Functional Materials, School of Physics and Electronic Engineering, Jiangsu Normal University, 221116, Xuzhou, People's Republic of China

²Lawrence Livermore National Laboratory, Physical and Life Sciences Directorate, Livermore, California 94550, USA

³Department of Physics and Astronomy, High Pressure Science and Engineering Center, University of Nevada, Las Vegas, NV 89154, USA

⁴Department of Earth Sciences, UCL, Gower Street, London, WC1E 6BT, UK

(Dated: May 8, 2019)

van der Waals (vdW) layered compounds provided a fruitful research stage for realization of superconductivity. However, an vdW layered superconductor with a high transition temperature (T_c) at ambient conditions is still rare. Here, using variable-composition evolutionary structure predictions, we systematically explored the stable compounds in the P-S system up to 20 GPa. Opposed to the complex stoichiometries at ambient condition, only one compound, PS₂, is predicted to be thermodynamically stable above 8 GPa. Strikingly, PS₂ is a vdW layered material isostructural to 3R-MoS₂ exhibiting a predicted T_c of around 11 K at ambient pressure, both in the bulk and the monolayer form. PS₂ has been successfully synthesized via high-pressure experiments in excellent agreement with the theoretical predictions. This enables replacing transition metals with group V elements in transition metal dichalcogenides and paves the way in the search for new vdW layered materials with superior properties.

vdW layered materials such as graphite, black phosphorus, and transition metal dichalcogenides (TMDs) have attracted extensive interest due to the weak interlayer interactions that make them easily exfoliable [1–5]. The electronic properties, such as superconductivity, can change dramatically upon reduction from bulk to 2D and can effectively be tailored by an external field or charge-carrier doping [3–8]. Recently, superconductivity for the vdW layered compounds has been extensively investigated [4–8]. At ambient pressure conditions, the majority of vdW layered materials are semiconductors while few of them show metallic or semimetallic behaviors. For semiconducting vdW layered materials, superconductivity can be induced by chemical intercalation, external pressure, and electrostatic gating [9–17]. In the TMD family, there is a strong competition between charge density wave (CDW) and superconductivity. The transition from CDW state to superconducting state can be triggered by the external stimulus, as observed in TiSe₂ [12], MoS₂ [15], and MoTe₂ [14]. Bulk MoS₂ exhibits superconductivity with a T_c of ~12 K at ultrahigh pressure of 120 GPa [13]. Thin film MoS₂ becomes superconducting when it is heavily gated to the conducting regime, in which T_c reaches 10 K at optimal gating [15]. Electrostatically induced superconductivity has also been realized in thin films of 2H-WS₂ [16] and 2H-MoSe₂ [17]. For semimetallic vdW materials, superconductivity has been observed in Weyl semimetal MoTe₂ but with low T_c values (~0.1 K) under ambient conditions [14]. Upon compression, the T_c of MoTe₂ dramatically increases to a maximum value of 8.2 K at 11.7 GPa accompanied by a 1T'-to-2H polytype transformation [14]. Metallic 2H-NbSe₂, a record holder in intrinsic superconducting TMDs, exhibits a transition temperature of 7.2 K at ambient conditions [18].

Economically, it is also valuable to replace transition metals in TMD materials with more abundant and inexpensive main group elements. Group IVA chalcogenides have attracted great attention because of their emergent physics phenom-

ena such as surface state, quantum spin Hall effects, and superconductivity [19]. SnSe₂ has been reported to become superconducting by organometallic intercalation [20], physical gating [19], and external pressure [21]. Recently, Zeng *et al* induced a superconductivity state ($T_c \approx 3.9$ K) in 1T-SnSe₂ by using the ionic liquid gating technique [19]. It was also reported that 1T-SnSe₂ exhibits robust superconductivity with a nearly constant $T_c \approx 6.1$ K between 30.1 and 50.3 GPa [21].

In recent years, the search for layered vdW materials that exhibit superconductivity has intensified [6–8]. In this letter, we report that phosphorus and sulfur, two neighboring elements in the periodic table, can form an unexpectedly stable layered compound PS₂ under relatively low-pressure conditions. Following this prediction, PS₂ was confirmed by performing high-pressure experiments in a laser-heated diamond anvil cell (LHDAC), starting from an elemental P-S mixture. The synthesized compound was characterized via *in situ* synchrotron X-ray diffraction (XRD) and Raman spectroscopy measurements. PS₂ is predicted to be superconducting with a transition temperature (~11.3 K) comparable to that (11.5 K) of CaC₆ at ambient pressure [10].

The *ab initio* evolutionary algorithm USPEX [22, 23] was used to explore thermodynamically stable P-S compounds and their structures. In these calculations, all stoichiometries were allowed (with the constraint that the total number of atoms in the unit cell is no more than 32 atoms), and calculations were performed at 1, 5, 10, and 20 GPa, respectively. The pressure-composition phase diagram of the P-S system is shown in Fig. 1 and Supplemental Fig. S1 [24], in which the convex hull was constructed from the normalized formation enthalpies of all the stable structures for each pressure. Thermodynamically, the convex hull at a given pressure connects all stable phases against decomposition into other binaries or elements. We first considered the phase transitions on two ending members (elemental P and S). Phosphorus transforms from the orthorhombic A17 structure (*Cmca*) to the

rhombohedral $A7$ phase ($R\bar{3}m$) to the simple cubic phase in the pressure range considered [25, 26], whereas sulfur in this pressure range undergoes a series of phase transitions from $Fddd$ to $P3_221$ to $R\bar{3}$ and to $I4_1/acd$ [27–29]. Using variable-composition evolutionary searches, we found that the P-S system holds a richer phase diagram at pressures lower than 3 GPa. Four previously reported compounds with discrete cage-like molecules, P_4S_3 [30], P_4S_7 [31], P_4S_9 [32], and P_2S_5 [31] (Supplemental Fig. S2) [24], are thermodynamically stable at zero pressure within a narrow pressure range: P_4S_3 (< 2 GPa); P_4S_7 (< 6 GPa); P_4S_9 (< 1 GPa), and P_2S_5 (< 2 GPa). The reported phosphorous polysulfide, P_2S_7 [33] with neutral polymeric strands, is thermodynamically stable one from 1 GPa to 8 GPa. Surprisingly, an unreported compound PS_2 is found to be the only compound thermodynamically stable above 8 GPa as shown in Fig. 1 and Fig. S3 [24]. Below 8 GPa, PS_2 is metastable compound. We also performed the phonon dispersion curves for PS_2 at a series of pressures (Fig. S4) [24]. The absence of imaginary phonon frequencies confirmed its dynamical stability within the entire range of pressure.

As shown in Fig. 2(a), PS_2 is a layered vdW solid isostructural to $3R$ - MoS_2 , belonging to D_{3d} ($R\bar{3}m$) space group [34, 35]. Its unit cell is composed of three phosphorous atoms occupying 3a Wyckoff sites (0, 0, 0) and six sulfur atoms at 6c (0, 0, z). We mention that MoS_2 has two different forms of $3R$ polytypes: one is the $CdCl_2$ -type structure (space group $R\bar{3}m$) with inversion symmetry [34, 35] which occurs in γ - TaS_2 [35] and β - $TaSe_2$ [35] as well as our PS_2 , another is the $R3m$ structure with broken inversion symmetry which is well-known in the TMDs family [4, 35, 36]. Considering that layered TMDs exhibit a variety of polytypes [2–4, 14] such as $2H$, $1T$, $1T'$, and T_d , we also examined the possibility of these structures occurred in PS_2 . Our DFT calculations suggested $3R$ - MoS_2 with $R\bar{3}m$ symmetry is indeed the ground state among these polytypes [24]. In addition, in order to evaluate the influences of interlayer vdW interaction on structural parameters of PS_2 [24], we considered the SCAN+rVV10 method [37], which can produce excellent interlayer spacing and intralayer lattice constants. The calculated lattice parameters are 3.258 Å for a and 17.344 Å for c at ambient conditions, which yields the density of 2.971 g/cm³ and the interlayer spacing of 5.782 Å. The optimized internal free parameter z is 0.256. PS_2 holds a slightly lower interlayer spacing than that (6.15 Å) of $3R$ - MoS_2 [34].

In order to verify the theoretical predictions and explore the pressure range of the stability of PS_2 , we performed LHDAC experiments (Fig. S5 [24]) on the phosphorous-sulfur mixture at various pressures, from 10 to 20 GPa and temperatures, from 800 K to 2000 K. All synthesis experiments concluded the formation of the layered PS_2 compound independently of the starting pressure, the maximum achieved temperature and the presence or not of thermal insulation (LiF). This observation agrees with the theoretical prediction that the layered PS_2 is the only thermodynamically stable composition above 8 GPa. In Fig. 2(b) we show the XRD patterns ($\lambda = 0.4959$

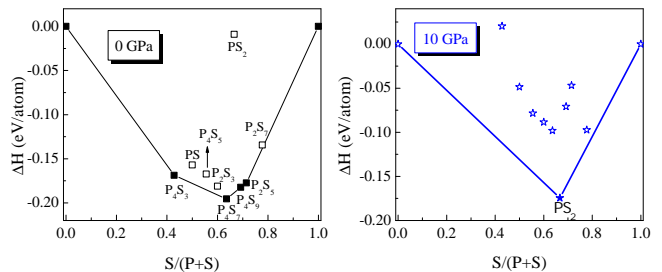


FIG. 1. The predicted convex hull diagrams in P-S system at the pressure of 0 GPa and 10 GPa.

Å) acquired during a synthesis attempt at 14 GPa. The XRD pattern before LH at room temperature (RT) is representative of a heterogeneous mixture of orthorhombic sulfur (S-I) and simple cubic phosphorous (SC-P). As expected, amorphous red phosphorous converts to the corresponding crystal structures of black phosphorous above 7 GPa [38, 39]. The corresponding cell volumes are in excellent agreement with previous high-pressure equation of state (EOS) studies of sulfur and phosphorous [26, 28]. New narrow Bragg peaks appear after LH (see Fig. 2(b)), while the Bragg peaks of S-I disappear and the ones of SC-P become narrower due to temperature annealing. The new Bragg peaks can be indexed with a mixture of the predicted PS_2 structure and tetragonal S-III. According to previous studies, at elevated pressure S-I transform to tetragonal S-III at temperatures below the temperatures achieved by LH in this study and S-III is quenchable at ambient temperature [29]. Bragg peaks of S-III were indexed with $a = 8.423$ Å and $c = 3.521$ Å at 14 GPa in excellent agreement with Ref. [29]. The remaining Bragg peaks can be indexed with the $R3m$ - PS_2 with $a = 3.149$ Å and $c = 15.501$ Å in good agreement with the theoretically predicted values ($a = 3.120$ Å and $c = 15.231$ Å at 14 GPa). A representative Le Bail refinement ($\lambda = 0.3344$ Å) is shown in the Supplemental Fig. S6 [24].

With decreasing pressure, the newly synthesized phase remains stable down to 4 GPa, as evidenced from XRD measurements and optical observations. Below this pressure the XRD patterns is representative of a mixture of crystalline P and a disordered-like (broad Bragg peaks) phase. It is plausible to assume that this disordered phase is the disordered metastable phase of sulfur previously observed on pressure release of S-III by Degtyareva *et al.* [29]. Thus, we conclude that PS_2 decomposes to P+S below 3 GPa. However, our phonon calculations suggested that PS_2 should be quenchable to the ambient condition. The observed decomposition may be a result of small grain size and large ratio of interfaces, which to some extent reduce the decomposition barrier. Pressure dependence of the lattice parameters and EOS of PS_2 together with the theoretically predicted ones are shown in Fig. 2(c). Experiment and theory agree closely for the lattice parameters and the cell volume. In particular, the experimental and theoretical unit cell volumes differ by less than 4 %, which is

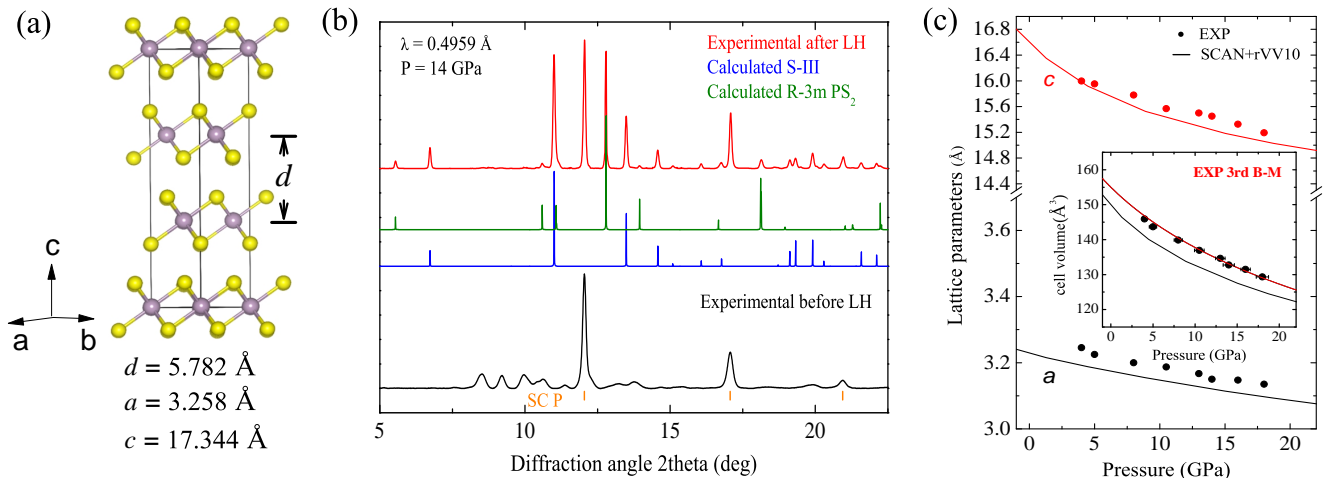


FIG. 2. (a) The crystal structure of vdW layered compound PS_2 . The lattice parameters a and c and interlayer spacing d at zero pressure given. (b) Integrated XRD patterns before laser heating (LH) and after LH to 800 K, respectively. Vertical ticks correspond to expected (assuming continuous Debye rings, see supplementary materials [24]) positions and intensities of XRD peaks of SC-P, S-III and PS_2 . (c) Pressure dependence of lattice parameters of PS_2 . The inset shows the pressure dependence of the cell volume. Experimental data are shown with solid symbols and theoretical predictions with solid lines. The solid red curve in inset is the third-order Birch-Murnaghan (3rd B-M) equation of states fit to the experimental data.

within the expected accuracy of DFT calculations [40]. We conducted EOS fits to the experimental and calculated PV data using a third-order Birch-Murnaghan EOS and determined the bulk modulus B_0 and the first derivative B_0' [41]. The results of the fits are $V_0 = 152.5 (7) \text{ \AA}^3$, $B_0 = 78.7(15) \text{ GPa}$, $B_0' = 4.0 (5)$, for the experimental EOS and $V_0 = 149.5 \text{ \AA}^3$, $B_0 = 56.5 \text{ GPa}$, $B_0' = 5.9$ for the calculated one.

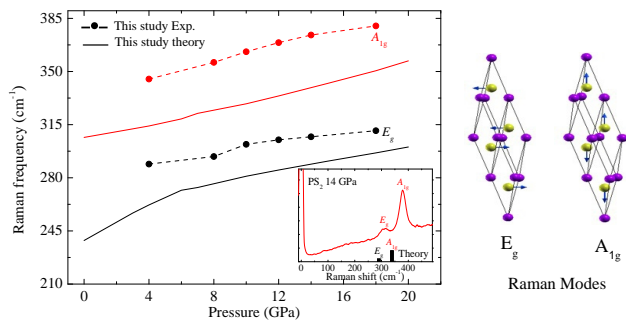


FIG. 3. Frequencies of Raman modes of PS_2 against pressure upon decompression. Experimental results with solid symbols and theoretically predicted with solid lines. The inset shows the experimental Raman spectrum at 14 GPa in comparison with the theoretically predicted Raman modes. Eigenvectors of Raman modes E_g and A_{1g} as the inset also given.

For PS_2 , there are four distinct optical phonon modes at the zone center: two Raman active modes E_g (two-fold degeneracy, S in-plane, basal plane vibrations) and A_{1g} (S out-of-plane, along c -axis vibrations) along with two infrared active modes E_u (two-fold degeneracy, in-plane S and P displacements) and A_{2u} (out-of-plane S and P displacements) (see the Fig. 3 and Fig. S7 [24]). The Raman spectrum, using the

514.5 nm line of an Ar ion laser for excitation, of the new phase depicted in Fig. 3 shows the presence of two distinct Raman active modes. Relative intensity and frequency separation of the modes allowed us to confidently assign the two modes to the A_{1g} (higher intensity/frequency) and E_g (lower intensity/frequency) of the layered PS_2 compound. Upon pressure release both modes show normal mode behavior (red shift) and can be traced down to 3~4 GPa in agreement with XRD measurements. Experimental Raman modes frequencies and frequency-pressure slopes are in good agreement with the theoretically calculated ones, given the fact that GGA underestimates the phonon frequencies [42].

The distinctive layered features in PS_2 aroused our intense interests in exploring its electronic properties. Remarkably, PS_2 is predicted to be a phonon-mediated superconductor even at zero pressure. The energy bands of PS_2 at 3 GPa are shown in Fig. 4(a). There is only one energy band crossing the Fermi level along several high symmetry directions in the Brillouin zone (BZ, see Fig. 4(b)). The most interesting feature is the presence of nearly flat bands lying right at the Fermi level along B_1 -B and XQ directions in the BZ. The occurrence of flat and steep slopes near the Fermi level resembles a favorable condition for enhancing Cooper pair formation, which is essential to phonon-mediated superconductivity [43]. The calculated density of states (DOS) shows that there is a strong hybridization between the S- p and P- s electrons in the whole BZ, indicating that these electrons dominate the electronic properties of PS_2 . As shown in Fig. 4(c), the Fermi surface (FS) of the PS_2 consists of a small electron-like pocket around Γ point and six linked electron-hole tubes (nearly elliptical sections) with a large surface area running through the BZ borders along the Γ -Z direction, exhibiting an evident

2D behavior. The existence of nearly parallel pieces of the F-S is beneficial to the electron-phonon coupling.[44] Both the Fermi pockets and the obvious Fermi nesting lead to strong electron-phonon interactions in PS₂.

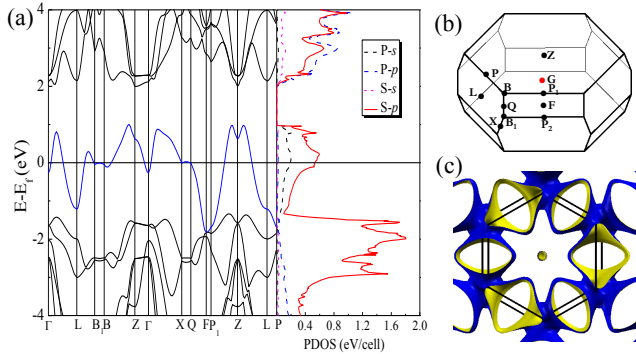


FIG. 4. Energy band, projected electronic density of states (PDOS) (a), Brillouin zone (b), and Fermi surface (c) of PS₂ at 3 GPa. The Fermi level was taken as the energetic reference point.

The phonon dispersion curve, partial atomic phonon DOS, Eliashberg spectral function $\alpha^2F(\omega)$, and integrated $\lambda(\omega)$ of PS₂ at 3 GPa are shown in Fig. 5. To gain further insights into the nature of electron-phonon coupling, the linewidths for phonon mode $\mathbf{q}\nu$ (i.e., $\gamma_{\mathbf{q}\nu}$) were attached to phonon dispersion curves. One can identify the contribution to the electron-phonon coupling strength from each phonon mode based on the calculated phonon linewidths. The softening of the E_g branch is observed along the X- Γ -L, B-Z, and P₁-Z-L directions, signaling again strong electron-phonon coupling in PS₂. Such a softening of the mode was previously observed in the superconducting MgB₂ [45]. Combining the calculated phonon linewidths with electronic structure, we conclude that the E_g modes are strongly coupled to electronic bands from S- p_x and S- p_y as well as P- s states since E_g modes involve atomic displacements in the x - y plane. Delta-like peak around 251 cm⁻¹ in both spectral function $\alpha^2F(\omega)$ and phonon DOS originates mostly from the E_g modes with calculated energies in the ranges of 207 to 257 cm⁻¹, which contributes to 33.3 % of the total λ value. The A_{1g} branch possess energies in the ranges of 292 to 371 cm⁻¹ and holds the highest phonon linewidth around Γ point. However, it contributes to only 3.1 % of the total λ value because of strong anisotropy of the line width of A_{1g} branch in the BZ. These results indicate that the sulfur atoms dominate superconductivity in PS₂, due to the prominent contributions to the electron-phonon interaction. Phonons from the sulfur atoms together with the electrons from the S- p and P- s states provide the strong electron-phonon coupling indispensable for superconductivity in PS₂.

From the value of λ , one can estimate the T_c using the Allen and Dynes formula [46]. Taking a typical value of 0.11 for μ^* along with the calculated ω_{\log} of 235 cm⁻¹, we obtained a T_c of 11.3 K for PS₂ at zero pressure. The changes of λ , ω_{\log} , and T_c with increasing pressure in PS₂ are depicted in Fig. 6. Applying pressure on PS₂ clearly leads to a significant

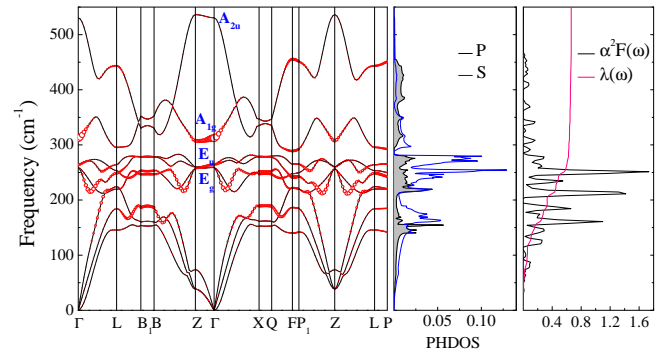


FIG. 5. Phonon spectrum, in which the linewidths for phonon mode $\mathbf{q}\nu$ (i.e., $\gamma_{\mathbf{q}\nu}$) are represented by the area of the red circle, partial atomic phonon DOS, Eliashberg spectral function $\alpha^2F(\omega)$ and integrated $\lambda(\omega)$ for PS₂ at the pressure of 3 GPa.

decrease of λ and T_c . At 20 GPa, T_c is only 2.4 K. The sharp drop of λ is closely associated with the decrease of DOS at the Fermi level because the Fermi level moves up as the pressure increases.

The single or few-layered thick, two-dimensional (2D) crystals are particularly interesting due to their potential use in low dimensional electronics [2, 5, 8]. Therefore, it is interesting to discuss the superconductivity of the monolayer PS₂. Compared with bulk superconductors, 2D superconductors are more convenient for fabrication in modern electronic applications. So far, the well-defined 2D intrinsic superconductors were rarely reported. For TMDs, only monolayer 2H-NbSe₂ [47] were found to exhibit intrinsic superconductivity with a relatively lower transition temperature (below 3 K) than that of its bulk counterpart (7.2 K) [18, 48, 49]. The weakened superconductivity due to the reduction of the dimensionality is a universal behavior in the TMD family except TaS₂ [50]. For our PS₂, the superconductivity also persisted from bulk to monolayer. Different from the NbSe₂, we surprisingly found that **at ambient pressure** the monolayer PS₂ has a slightly lower T_c (about 10.8 K) than bulk **because of a slightly lower coupling constant (about 0.8) than bulk**, indicating that bulk PS₂ could be an ideal 2D superconductor.

In conclusion, we report a novel layered PS₂ compound from a joint effort between theory and experiment. Our complete survey on the pressure-composition phase diagram for the P-S system at pressures up to 20 GPa yielded a novel compound PS₂ to become thermodynamically stable above 8 GPa. PS₂ is **predicted to be** an unusual example of superconducting vdW layered material, **exhibiting superconductivity** with an unexpected high transition temperature (~ 11.3 K) at ambient conditions. Monolayer PS₂ retains the superconducting property of bulk PS₂, suggesting that PS₂ is an ideal candidate material for exploring 2D superconductivity. Experimental results, from diffraction and spectroscopic techniques, unambiguously identified the synthesized compounds as the predicted layered $R\bar{3}m$ -PS₂. We believe the discovery of non-intuitive vdW layered compound between group V and

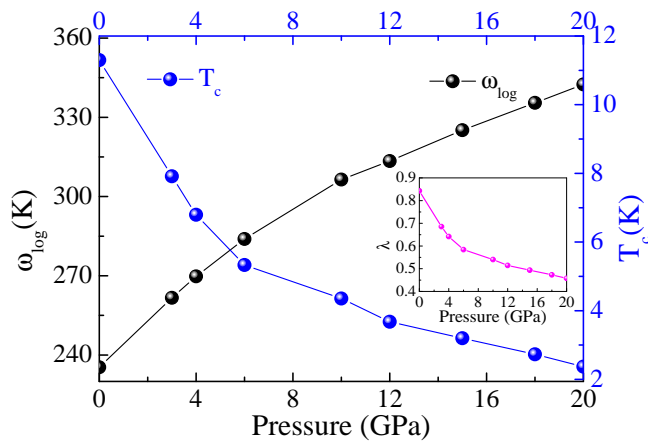


FIG. 6. Calculated T_c values and logarithmic phonon momentum ω_{\log} versus pressure. Inset shows the integrated electron-phonon coupling λ as a function of pressure.

VI elements will opens a new avenue in vdW layered materials design.

We acknowledge supports from the National Natural Science Foundation of China (Grant No. 11674131) and the 333 project of Jiangsu province. Part of this work was performed under the auspices of the U. S. Department of Energy by Lawrence Livermore National Security, LLC under Contract DE-AC52-07NA27344. We gratefully acknowledge the LLNL LDRD program for funding support of this project under 18-LW-036. Part of this work was performed at GeoSoilEnviroCARS (The University of Chicago, Sector 13), Advanced Photon Source (APS), Argonne National Laboratory. GeoSoilEnviroCARS is supported by the National Science Foundation-Earth Sciences (EAR-1634415) and Department of Energy-GeoSciences (DE-FG02-94ER14466). This research used resources of the Advanced Photon Source, a U. S. Department of Energy (DOE) Office of Science User Facility operated for the DOE Office of Science by Argonne National Laboratory under Contract No. DE-AC02-06CH11357. The ALS is supported by the Director, Office of Science, BES of DOE under Contract No. DE-AC02-05CH11231, DE-AC02-06CH11357.

Y. L. L and E. S. contributed equally to this work.

* ylli@jsnu.edu.cn

- [1] X. Qiu and W. Ji, Illuminating interlayer interactions, *Nat. Mater.* **17**, 211 (2018).
- [2] A. V. Kolobov and J. Tominaga, *Two-Dimensional Transition-Metal Dichalcogenides* (Springer, 2016).
- [3] H. Yang, S. Kim, M. Chhowalla, and Y. Lee, Structural and quantum-state phase transition in van der Waals layered materials, *Nat. Phys.* **13**, 931 (2017).
- [4] G. H. Han, D. L. Duong, D. H. Keum, S. J. Yun, and Y. H. Lee, van der Waals metallic transition metal dichalcogenides, *Chem. Rev.* **118**, 6297 (2018).

- [5] S. Manzeli, D. Ovchinnikov, D. Pasquier, O. V. Yazyev, and A. Kis, 2D transition metal dichalcogenides, *Nat. Rev. Mater.* **2**, 15. 17033 (2017).
- [6] R. P. Smith, T. E. Weller, C. A. Howard, M. P. Dean, K. C. Rahnejat, S. S. Saxena, and M. Ellerby, Superconductivity in graphite intercalation compounds, *Physica C* **514**, 50 (2015).
- [7] R. A. Klemm, Pristine and intercalated transition metal dichalcogenide superconductors, *Physica C* **514**, 86 (2015).
- [8] Y. Saito, T. Nojima, and Y. Iwasa, Highly crystalline 2D superconductors, *Nat. Rev. Mater.* **2**, 16094 (2016).
- [9] G. Csányi, P. B. Littlewood, A. H. Nevidomskyy, C. J. Pickard, and B. D. Simons, The role of the interlayer state in the electronic structure of superconducting graphite intercalated compounds, *Nat. Phys.* **1**, 42 (2005).
- [10] N. Emery, C. Hérod, M. d'Astuto, V. Garcia, C. Bellin, J. F. Marêché, P. Lagrange, and G. Loupías, Superconductivity of bulk CaC_6 , *Phys. Rev. Lett.* **95**, 087003 (2005).
- [11] A. Gauzzi, S. Takashima, N. Takeshita, C. Terakura, H. Takagi, N. Emery, C. Hérod, P. Lagrange, and G. Loupías, Enhancement of superconductivity and evidence of structural instability in intercalated graphite CaC_6 under high pressure, *Phys. Rev. Lett.* **98**, 067002 (2007).
- [12] E. Morosan, H. W. Zandbergen, B. S. Dennis, J. W. G. Bos, Y. Onose, T. Klimczuk, A. P. Ramirez, N. P. Ong, and R. J. Cava, Superconductivity in Cu_xTiSe_2 , *Nat. Phys.* **2**, 544 (2006).
- [13] Z. Chi, X. Chen, F. Yen, F. Peng, Y. Zhou, J. Zhu, Y. Zhang, X. Liu, C. Lin, S. Chu, Y. Li, J. Zhao, T. Kagayama, Y. Ma, and Z. Yang, Superconductivity in pristine $2\text{H}_a\text{-MoS}_2$ at ultrahigh pressure, *Phys. Rev. Lett.* **120**, 037002 (2018).
- [14] Y. Qi *et al.*, Superconductivity in Weyl semimetal candidate MoTe_2 , *Nat. Commun.* **7**, 11038 (2016).
- [15] J. T. Ye, Y. J. Zhang, R. Akashi, M. S. Bahramy, R. Arita, and Y. Iwasa, Superconducting dome in a gate-tuned band insulator, *Science* **338**, 1193 (2012).
- [16] S. Jo, D. Costanzo, H. Berger, and A. F. Morpurgo, Electrostatically induced superconductivity at the surface of WS_2 , *Nano Lett.* **15**, 1197 (2015).
- [17] W. Shi, J. Ye, Y. Zhang, R. Suzuki, M. Yoshida, J. Miyazaki, N. Inoue, Y. Saito, and Y. Iwasa, Superconductivity series in transition metal dichalcogenides by ionic gating, *Sci. Rep.* **5**, 12534 (2015).
- [18] T. Yokoya, T. Kiss, A. Chainani, S. Shin, M. Nohara, and H. Takagi, Fermi surface sheet-dependent superconductivity in 2H-NbSe_2 , *Science* **294**, 2518 (2001).
- [19] J. Zeng *et al.*, Gate-induced interfacial superconductivity in 1T-SnSe_2 , *Nano Lett.* **18**, 1410 (2018).
- [20] D. O'Hare, H.-V. Wong, S. Hazell, and J. W. Hodby, Relatively isotropic superconductivity at 8.3 K in the lamellar organometallic intercalate $\text{SnSe}_2\{\text{Co}(\eta\text{-C}_5\text{H}_5)_2\}_{0.3}$, *Adv. Mater.* **4**, 658 (1992).
- [21] Y. Zhou *et al.*, Pressure-induced metallization and robust superconductivity in pristine 1T-SnSe_2 , *Adv. Electron. Mater.* **4**, 1800155 (2018).
- [22] A. R. Oganov and C. W. Glass, Crystal structure prediction using ab initio evolutionary techniques: Principles and applications, *J. Chem. Phys.* **124**, 244704 (2006).
- [23] A. O. Lyakhov, A. R. Oganov, H. T. Stokes, and Q. Zhu, New developments in evolutionary structure prediction algorithm USPEX, *Comp. Phys. Comm.* **184**, 1172 (2013).
- [24] See Supplemental Material at http://link.aps.org/**** for a detailed description of theoretical calculations and experimental methods, convex hull, crystal structures, phonon spectrum, Le Bail refinement, XRD patterns, and structural parameters of PS_2 using different vdW corrections.

- [25] J. C. Jamieson, Crystal structures adopted by black phosphorus at high pressures, *Science* **139**, 1291 (1963).
- [26] T. Kikegawa and H. Iwasaki, An X-ray diffraction study of lattice compression and phase transition of crystalline phosphorus, *Acta Cryst.* **B39**, 158 (1983).
- [27] J. Donohue, A. Caron, and E. Goldish, The crystal and molecular structure of S_6 (Sulfur-6), *J. Am. Chem. Soc.* **83**, 3748 (1961).
- [28] Y. Akahama, M. Kobayashi, and H. Kawamura, Pressure-induced structural phase transition in sulfur at 83 GPa, *Phys. Rev. B* **48**, 6862 (1993).
- [29] O. Degtyareva, E. Gregoryanz, M. Somayazulu, P. Dera, H.-k. Mao, and R. J. Hemley, Novel chain structures in group VI elements, *Nat. Mater.* **4**, 152 (2005).
- [30] G. R. Burns, J. R. Rollo, and R. W. Syme, Raman spectra of single crystals of α - P_4S_3 , *J. Raman Spectrosc.* **19**, 345 (1988).
- [31] A. Vos, R. Olthof, F. Van Bolhuis, and R. Botterweg, Refinement of the crystal structures of some phosphorus sulphides, *Acta Cryst.* **19**, 864 (1965).
- [32] W. Hilmer, Die struktur eines phosphor (III, V)-sulfids der ungefähren zusammensetzung P_4S_9 , *Acta Cryst.* **B25**, 1229 (1969).
- [33] T. Rödl, R. Wehrich, J. Wack, J. Senker, and A. Pfitzner, Rational syntheses and structural characterization of sulfur-rich phosphorus polysulfides: α - P_2S_7 and β - P_2S_7 , *Angew. Chem. Int. Ed.* **50**, 10996 (2011).
- [34] R. E. Bell and R. E. Herfert, Preparation and characterization of a new crystalline form of molybdenum disulfide, *J. Am. Chem. Soc.* **79**, 3351 (1957).
- [35] F. Lévy (Ed.), *Crystallography and Crystal Chemistry of Materials with Layered Structures* (Reidel, 1976).
- [36] R. Suzuki *et al.*, Valley-dependent spin polarization in bulk MoS_2 with broken inversion symmetry, *Nat. Nanotech.* **9**, 611 (2014).
- [37] H. Peng, Z.-H. Yang, J. P. Perdew, and J. Sun, Versatile van der Waals density functional based on a meta-generalized gradient approximation, *Phys. Rev. X* **6**, 041005 (2016).
- [38] J. M. Zaugg, A. K. Soper, and S. M. Clark, Pressure-dependent structures of amorphous red phosphorus and the origin of the first sharp diffraction peaks, *Nat. Mater.* **7**, 890899 (2008).
- [39] E. Rissi, E. Soignard, K. McKiernan, C. Benmore, and J. Yarger, Pressure-induced crystallization of amorphous red phosphorus, *Solid State Commun.* **152**, 390 (2012).
- [40] Y. L. Li, S. N. Wang, A. R. Oganov, H. Gou, J. S. Smith, and T. A. Strobel, Investigation of exotic stable calcium carbides using theory and experiment, *Nat. Commun.* **6**, 6974 (2015).
- [41] F. Birch, Finite strain isotherm and velocities for single-crystal and polycrystalline NaCl at high pressures and 300 K, *J. Geophys. Res.* **83**, 1257 (1978).
- [42] F. Favot and A. Dal Corso, Phonon dispersions: Performance of the generalized gradient approximation, *Phys. Rev. B* **60**, 11427 (1999).
- [43] Y. L. Li, W. Luo, Z. Zeng, H. Q. Lin, H. k. Mao, and R. Ahuja, Pressure-induced superconductivity in CaC_2 , *Proc. Natl. Acad. Sci.* **110**, 9289 (2013).
- [44] Y. L. Li, W. Luo, X. J. Chen, Z. Zeng, H. Q. Lin, and R. Ahuja, Formation of nanofoam carbon and re-emergence of superconductivity in compressed CaC_6 , *Sci. Rep.* **3**, 3331 (2013).
- [45] A. Q. R. Baron, H. Uchiyama, Y. Tanaka, S. Tsutsui, D. Ishikawa, S. Lee, R. Heid, K.-P. Bohnen, S. Tajima, and T. Ishikawa, Kohn anomaly in MgB_2 by inelastic X-ray scattering, *Phys. Rev. Lett.* **92**, 197004 (2004).
- [46] P. B. Allen and R. Dynes, Transition temperature of strong-coupled superconductors reanalyzed, *Phys. Rev. B* **12**, 905 (1975).
- [47] M. Ugeda *et al.*, Characterization of collective ground states in single-layer $NbSe_2$, *Nat. Phys.* **12**, 92 (2016).
- [48] X. Xi, Z. Wang, W. Zhao, J. Park, K. Law, H. Berger, L. Forró, J. Shan, and K. Mak, Ising pairing in superconducting $NbSe_2$ atomic layers, *Nat. Phys.* **12**, 139 (2016).
- [49] H. Wang *et al.*, High-quality monolayer superconductor $NbSe_2$ grown by chemical vapour deposition, *Nat. Commun.* **8**, 394 (2017).
- [50] E. Navarro-Moratalla *et al.*, Enhanced superconductivity in atomically thin TaS_2 , *Nat. Commun.* **7**, 11043 (2016).